Proceedings of the 12th International Conference on Fluid Flow, Heat and Mass Transfer (FFHMT 2025)
July 15, 2025 - July 17, 2025 | Imperial College London Conference, London, United Kingdom
Paper No. 166
DOI: 10.11159/ffhmt25.166

Dilute Viscoelastic Fluids for Enhanced Heat Transfer in Immersion Cooling Concepts

Joseph Rosenfeld[1], Mehdi Seddiq[1], Bastian Rüppel[2], Lukas Weiß[2], Hendrik Reese[3], Ioannis Karathanassis[1], Timothy Smith[4], Gareth Brown[4], Michael Wensing[2], Manolis Gavaises[1]
[1]City St George's, University of London
Northampton Square, London EC1V 0HB, United Kingdom
Joseph.Rosenfeld@city.ac.uk; ioannis.karathanassis@city.ac.uk
[2]Friedrich-Alexander-Universität
Erlangen-Nürnberg, Schloßplatz 4, 91054 Erlangen
[3]Otto-von-Guericke-University
Universitatsplatz 2, 39106 Magdeburg, Germany
[4]Lubrizol European Research and Development Centre
Nether Lane, Hazelwood, DE56 4AN Derby, United Kingdom

Abstract - Viscoelastic fluids are promising candidates for the thermal management of high heat-flux components of electrified powertrains, such as the battery pack via immersion cooling concepts. This study investigates the ability of viscoelasticity-inducing additives to manipulate flow patterns and enhance heat transfer in a benchmark bluff body geometry, under inertial laminar flows using dilute polymer solutions. Simulations were conducted in OpenFOAM to model viscoelastic fluid flow using the Phan-Thien-Tanner (PTT) constitutive equation and were validated against particle image velocimetry (PIV) experimental data. Two benchmark-flow configurations were studied: (i) a 180-degree channel bend and (ii) flow around a heated bluff body. Results show that viscoelastic fluids enhance vorticity in both geometries to varying extents compared to Newtonian fluids, as a function of the PTT-model slip (ζ) parameter. Heat transfer studies with a heated bluff body showed a trend of increasing heat flux for the viscoelastic fluid, with a measurable 3% enhancement at a Reynolds number of 800 also captured by the numerical results. The study highlights the potential of leveraging the influence of second normal stress difference in viscoelastic fluids for thermal management and discusses avenues for further optimisation.

Keywords**:** Heat transfer enhancement, wall-bounded flows, relaxation time, bluff body

1. Introduction

Immersion cooling using dielectric fluids has emerged as a method for enabling advanced electrification technologies via removal of heat transfer barriers and potentially simpler designs [1], [2], in comparison to the more common polar fluids and designs implemented [3], [4]. This becomes vital as demands for cleaner energy technologies increase [5], [6] and can avoid energy consuming materials commonly implemented in non-contact designs [7], [8]. The challenge to address with this technology is how to boost heat transfer as immersion coolants are necessarily dielectric and therefore possess a relatively low thermal conductivity [9].

Implementing passive mixing or secondary flows within a channel is a simple but powerful technique to enhance heat transfer from a heated surface [10]. One such method of inducing secondary flows is with the use of polymeric additives that generate normal forces that can facilitate mixing patterns near solid boundaries [11]. While there is a significant amount of literature on the relationship between fluid dynamics and polymeric additives in the turbulent regime [12] and the creeping flow to low-inertial regime [13], inertial laminar flows are a relatively unexplored region. It is unclear in this region whether vorticity patterns may be enhanced as in the creeping regime due to elastic forces [14], or if vorticity/secondary flow patterns may be suppressed via energy absorption and release as in the turbulent regime [15]. The complexity of this region lies in the interplay between elastic and inertial forces, with complex flow structures formed being termed elasto-inertial turbulence [16]. Elastic effects can generate complex secondary flow structures via gradients in the normal stress differences [11]. For numerous applications these flow conditions are of interest and the interplay between viscoelasticity and inertia remains relatively unexplored.

To investigate this, we employed a computational approach using the open-source CFD infrastructure OpenFOAM along with library RheoTool for viscoelasticity modelling [17]. The Phan-Thien-Tanner (PTT) constitutive model was employed as it takes second normal stress differences into account, critical for capturing secondary flows through gradients [18]. This study focuses on two benchmark flow geometries—flow through a 180-degree bend and flow around a bluff body. These configurations were chosen to explore how viscoelastic fluids influence vortical motion vortices, alter wake dynamics, and influence heat transfer, as they are simplistic representations of flows found in practical applications [19], [20]. Simulations are validated against particle image velocimetry (PIV) experiments and heat flux data with formulated viscoelastic fluids. This study bridges the gap between experimental and computational analysis, providing insights into the interplay of viscoelasticity, flow dynamics, and thermal performance.

2. Materials and Methods

2.1. Computational Methods

Two benchmark geometries are investigated in this study: a 180-degree bent tube (Figure 1A) and flow past a bluff body (Figure 1B). Grids consisting of 2.9 and 4.8 million cells for the curved tube and the bluff body respectively were found to be sufficient for resolving secondary flow pattern in the duct core but also the boundary layer region which is critical for heat-flux estimation in the bluff body geometry (Figure 1C). Unless otherwise specified, inlet velocity profiles are fully developed. For the series of bluff body simulations at a Reynolds number of 600, inlet velocity data is imported from experimentally measured values upstream of the bluff body to best match the velocity profiles for comparison. No slip is assumed at wall boundaries, and the outlet pressure is set to zero. The material properties for the fluids used in this study are listed in Table 1. To protect proprietary data, the polymer relaxation time for the viscoelastic sample is not listed. However, the Weissenberg number for flows in this study are ~ 10. For thermal studies, viscosity is adjusted according to an Arrhenius-type model, the product ρCp assumes a constant average value, the thermal conductivity is adjusted linearly with temperature, and the polymer relaxation time is assumed to be constant. Values given in Table 1 are the material properties at 40^{o}C, the inlet temperature set point. The PTT [18] viscoelastic constitutive equation is used to simulate viscoelastic flow behaviour, and the model parameters of ε and ζ are adjusted to see their effects on the flow profile. RheoTool incorporates buoyancy effects according to the Boussinesq approximation, as well as viscous dissipation. The viscoelastic constitutive equations are solved using the log-conformation approach, as this stabilises the solver against divergence [21]. An incompressible transient flow solver is employed for simulations. For the curved channel, isothermal flow at Reynolds number of 1200 was assumed and found to reach a steady state after a flow time of 0.2 seconds, thus data was extracted at that point. For the bluff body, isothermal flow was simulated for 1 second using a Courant number of 0.1, sampling data every 0.1 seconds for a total of ten data points, followed by solving the energy equation as well for 1 s with all surfaces of the bluff body set to a constant of 90 ^{o}C. Simulations were conducted in an HPC environment with runs requiring between 90-4,000 CPU hours. The governing equations solved for, are the conservation of mass and momentum for an incompressible fluid, as follows:

$$\nabla \cdot \mathbf{u} = 0 \tag{1}$$

$$\rho\left(\frac{\partial \boldsymbol{u}}{\partial t} + \boldsymbol{u} \cdot \nabla \boldsymbol{u}\right) = -\nabla P + \nabla \cdot \boldsymbol{\tau} \tag{2}$$

where ρ is the fluid density, **u** is the velocity vector, P is the pressure, and $\boldsymbol{\tau}$ is the stress tensor. The stress tensor is assumed to be a linear combination of the solvent and polymer contributions given by $\boldsymbol{\tau} = \boldsymbol{\tau}_S + \boldsymbol{\tau}_P$:

$$\boldsymbol{\tau}_S = \eta_S(\nabla \boldsymbol{u} + \nabla \boldsymbol{u}^T) \tag{3}$$

$$f(\boldsymbol{\tau}_P)\boldsymbol{\tau}_P + \lambda \overset{\blacksquare}{\boldsymbol{\tau}_P} = \eta_P(\nabla \boldsymbol{u} + \nabla \boldsymbol{u}^T) \tag{4}$$

$$f(\boldsymbol{\tau}_P) = \left(1 + \frac{\varepsilon\lambda}{\eta_P} tr(\boldsymbol{\tau}_P)\right) \ (Linear\ version\ of\ PTT\ model) \tag{5}$$

$$\overset{\blacksquare}{\boldsymbol{\tau}_P} = \frac{\partial \boldsymbol{\tau}}{\partial t} + \boldsymbol{u} \cdot \nabla \boldsymbol{\tau} - \boldsymbol{\tau} \cdot \nabla \boldsymbol{u} - \nabla \boldsymbol{u}^T \cdot \boldsymbol{\tau} + \zeta(\boldsymbol{\tau} \cdot \boldsymbol{D} + \boldsymbol{D} \cdot \boldsymbol{\tau}) \tag{6}$$

$$\boldsymbol{D} = \frac{1}{2}(\nabla \boldsymbol{u} + \nabla \boldsymbol{u}^T) \tag{7}$$

where subscript S denotes solvent contributions, P denotes polymer contributions, η is the viscosity (which is assumed to be a linear combination of solvent and polymer contributions), f is the destruction function representing network junction destructions, of which the linear version is shown here [22], λ is the polymer relaxation time, ε is a parameter that modifies the extensional properties of the fluid, ζ is referred to as the slip parameter [23], and **D** is the rate of deformation tensor. The PTT model is encapsulated by equations 4-7, and equation 6 is referred to as the Gordon-Schowalter derivative. The slip parameter ζ is important in that it represents the extent of the nonlinearity in the stress response to deformation and therefore is crucial in describing the behaviour of the fluid extensional viscosity. For non-isothermal flows, the energy equation is solved alongside the flow equations and is given by:

$$\rho Cp\left(\frac{\partial T}{\partial t} + \boldsymbol{u} \cdot \nabla T\right) = \nabla \cdot (k \nabla T) + \boldsymbol{\tau} : \nabla \boldsymbol{u} \tag{8}$$

where Cp is the fluid heat capacity, T is temperature, and k is thermal conductivity.

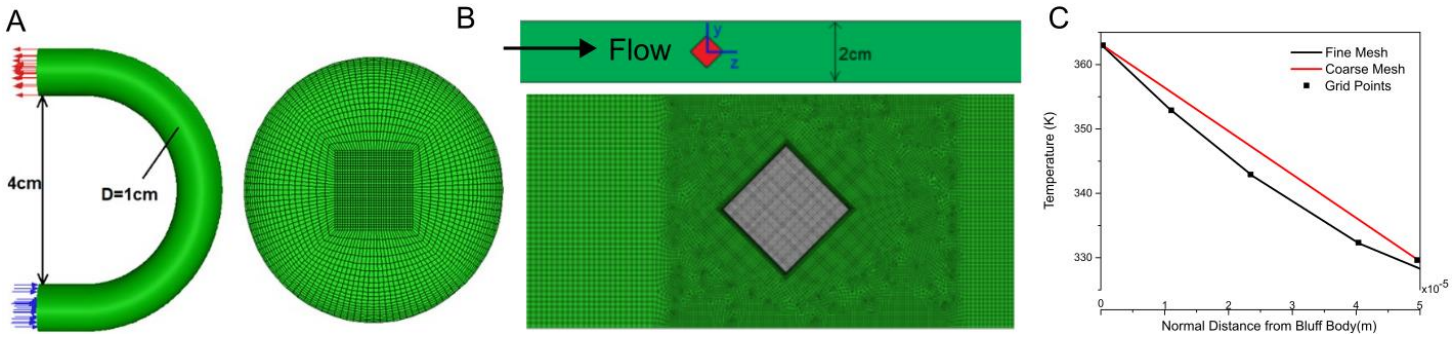

Fig. 1: Computational grids of geometries investigated in this work: A) 180deg bend and B) bluff body geometry. C) Representative temperature profile normal to the bluff body in the boundary layer region demonstrating accurate capture down to 10 μm.

2.2. Experimental Methods

Fluids are supplied by Lubrizol Ltd, and due to proprietary restrictions only essential material properties are included. Flow studies are conducted using PIV via suspending tracer particles in the respective fluids, flown through the same geometries as those described in Figure 1. Heat fluxes are measured using an atomic layer thermopile sensor [24] connected to the aluminium rod that acts as the bluff body. A detailed description of the experimental techniques can be found in [25].

Table 1: Fluid properties used in this study.

Name	Type	ρ (kg/m^3)	η_S (mPa·s)	η_P (mPa·s)	Cp (J/kg/K)	k (W/m/K)
Base Fluid	**Newtonian**	806	15.86	0	2191	0.1398
Viscoelastic	**Viscoelastic**	806	15.86	0.99	2190	0.1384

3. Results and Discussion

A parametric analysis of numerical predictions for variants of the PTT model is performed in this section in a comparative manner against experimental data for the two benchmark geometries examined. The rationale is to illustrate the influence of the PTT model parameters, corresponding to distinct rheological attributes of the viscoelastic fluid which are challenging to be measured with accuracy, on the predicted flow and temperature fields.

3.1. Isothermal flow in 180deg bend

The first geometry realises a 180-degree curved pipe, where at the apex centrifugal inertial forces act [26] inducing a secondary flow pattern consisting of a system of counter-rotating, so called, Dean vortices. This is illustrated in Figure 2A,

alongside a probe line offset 1.5 mm from the channel centre used to compare experimental and computational data. Hypothetically, under inertial laminar flows (Re = 1200), a Dean number of 240, and a Weissenberg number on the order of 10, we anticipate that there will be an interplay between inertial and elastic forces that will modify the vorticity profile accordingly. Figures 2B-2D graph the numerically and experimentally derived vorticity profiles for Newtonian (Figure 2B) and viscoelastic fluids (Figures 2C-D) and show that the simulations capture the secondary flow pattern accurately. In the case of viscoelastic flows, when both PTT model parameters (ε and ζ) are set to zero and only the polymer relaxation time is considered in the equations (collapsing the PTT model to the Oldroyd-B model [27]), simulations predict a significantly larger peak in vorticity, compared to experimental data. Interestingly, when either ε or ζ is varied even to values as small as $1x10^{-4}$, the vorticity peak is lowered and approaches the experimental value. This suggests reduced anisotropy in the stress tensor and corresponds to a specific, low negative, value of the second normal stress difference (N2), which on most occasions is challenging to be determined yet has a clear influence on the secondary flow behaviour of the viscoelastic fluids. The value range over which parameters ε and ζ are varied in line with values used in other studies [23], [28]. More interestingly, no further reduction in the vorticity peak is seen beyond a value of 0.01 for either parameter, and no distinct features are observed when both parameters are simultaneously nonzero.

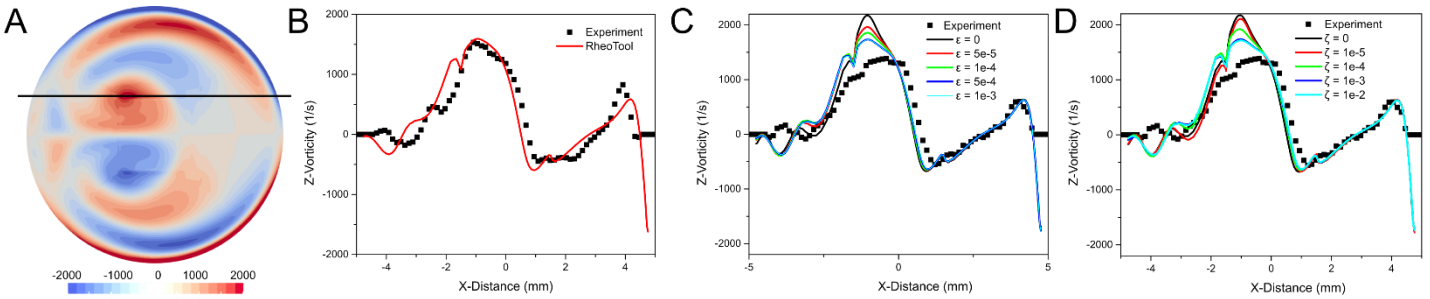

Figure 2: Results for 180-degree tube at Re = 1200: (A) Representative image of the Z-Vorticity component at the apex of the bend, revealing a system of multiple counter-rotating vortex pairs. The probe line shown at y = 1.5 mm above the center indicates the location for comparison to experimental results. (B) Voticity distribution along the probe line produced by simulations (solid line) and PIV data (markers) for the Newtonian fluid. (C) Vorticity distribution for the viscoelastic fluid produced with the PTT model, keeping ζ = 0 and comparison against PIV data. (D) Vorticity distribution for the viscoelastic fluid produced with the PTT model, keeping ε = 0 and comparison against PIV data.

3.2. Flow and heat transfer past a bluff body

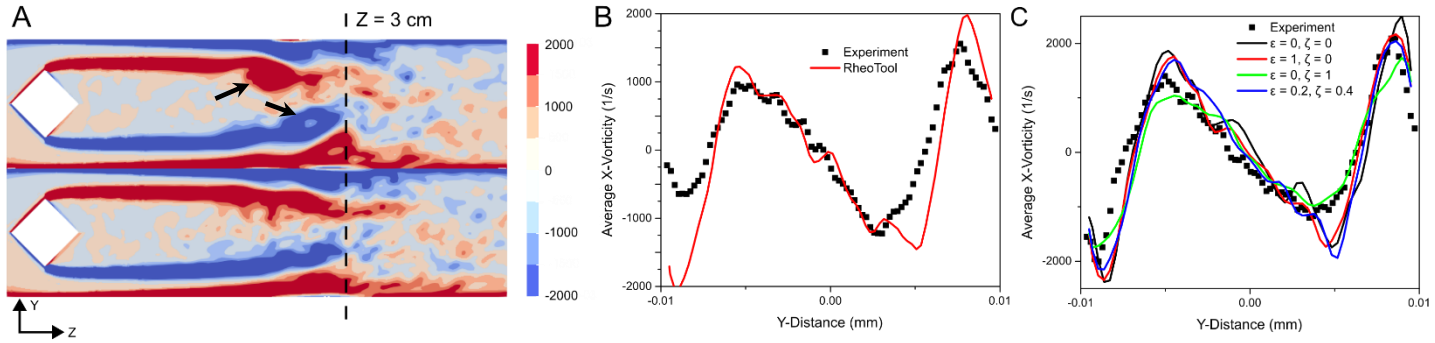

Fig. 3: Results for bluff body geometry at Re = 600. (A) Representative contour plot of X-Vorticity component, time averaged over 10 time steps for the Newtonian fluid (top) and the viscoelastic fluid (bottom). The probe line at Z = 3 cm is used to compare numerical against experimental data. (B) Comparison of the X-Vorticity distribution between experiment and simulation for the Newtonian fluid. (C) Same comparison for the viscoelastic fluid across a range of ε and ζ values.

When fluid flows past a bluff body in a wall bounded flow, a momentum boundary layer develops behind the bluff body resulting in vortex shedding [20]. In this geometry, we postulate that once again elastic forces generated from

polymeric motion will compete with inertial forces and will modify the downstream vorticity profile [29], [30], [31]. Figure 3A shows time-averaged vorticity contour plots for Newtonian and viscoelastic fluids, on an axial plane at the mid-height of the bluff body. Here we can clearly see the influence of viscoelasticity in interacting with the generated vortices. In the Newtonian plot, clear vortex loci can be detected (black arrows), with the positive and negative vortices curled up relative to each other. The plot, in essence, captures the time averaged representation of the vortical structures flapping motion. However, when a viscoelastic fluid is introduced at the same Reynolds number the average vorticity profile indicate that flapping is suppressed, and that vortex shedding occurs further downstream relative to the Newtonian fluid.

Figures 3B and 3C show the comparison of time-averaged experimental and computationally derived vorticity profiles at 3 cm downstream from the bluff body; this probe line acts as a fingerprint of the flow due to its more complex transient nature. Once again, numerical predictions are seen to capture qualitative and quantitative aspects of the flow for both the Newtonian and viscoelastic fluids. Here though, small value changes in the PTT model parameters did not affect the outcome of the simulation in a non-negligible manner, owing to the intrinsic nature of the flow with the specific geometrical layout inducing flow shearing over the elongation flow materialised in the curved tube. Therefore, variations are investigated at the end range of each parameter value, namely 0 to 1. When the ζ parameter is kept at zero and ε is varied across its range, the fit relative to experimental data is the most inaccurate, while when the ε parameter is set to zero and the ζ parameter is at a maximum, we qualitatively see the best fit across the full probe line, aligning closest with the peaks and valleys of the vorticity distribution. This may be due to the importance of the ζ parameter in capturing the second normal stress difference of the fluid [31]. When the parameters are both nonzero, a shift further from experimental data is seen, which suggests that the parameters can offset the effects of each other. Of note, when the ζ parameter is large suggests extensive overlapping of chains [32] which may occur when long polymers are used that are heavily stretched by fluid stresses [33].

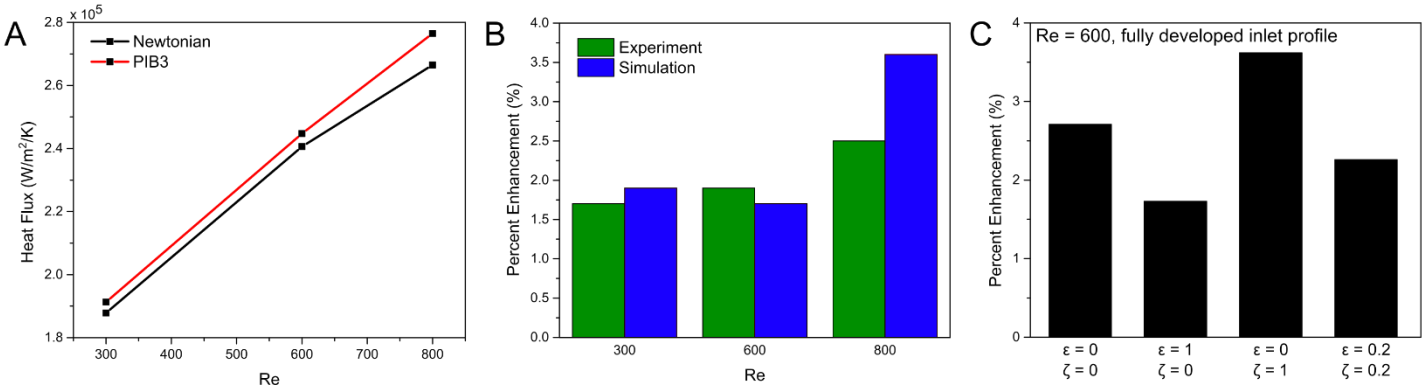

Fig. 4: Heat transfer on bluff body layout: (A) Surface-averaged heat flux across the bluff body for both Newtonian and viscoelastic fluids with PTT model parameters of ε = 0.2 and ζ = 0.2. (B) Heat flux enhancement of viscoelastic relative to Newtonian fluid for both experiment and simulation, with PTT model parameters of ε = 0.2 and ζ = 0.2. (C) A scan of the effects of the PTT parameters on the percent heat flux enhancement from the heated bluff body at Re = 600, and a fully developed inlet profile.

Vital for an immersion cooling application is understanding the effect of viscoelasticity on heat flux from a heated surface within the fluid. To study this computationally, the bluff body temperature is raised 50 C above the incoming fluid temperature, and the heat flux to the surrounding fluid is extracted. This boundary condition is employed to best match the energy input employed experimentally. Figure 4A shows the effect of varying the Reynolds number of the flow computationally on the heat flux from the bluff body to the fluid. It is shown that beyond a Reynolds number of 600, the viscoelastic fluid shows an increasing trend of higher heat flux relative to the Newtonian fluid. This may suggest that elasto-inertial instabilities induce greater passive mixing in boundary layer region leading to enhanced heat transfer. This trend is also captured in Figure 4B, where the modest yet measurable percent enhancement in heat flux of the viscoelastic fluid relative to the Newtonian fluid is demonstrated for both experiments and simulations. When the PTT model parameters are scanned for their effect on heat flux enhancement as shown in Figure 4C, we see that lower ε values and higher ζ values appear to promote heat flux enhancement. This is an interesting result alongside the vorticity profile comparison of Figure 3, where low ε and high ζ was closer in line with experimental results, and with regard to heat flux the same values promote higher heat transfer. This again stresses the importance of the ζ parameter as the generation of normal forces due to normal

stress gradients modifies the local vorticity field and is plausibly the underlying cause for the heat flux enhancement observed. These findings suggest that viscoelasticity can be strategically leveraged to enhance thermal performance in immersion cooling applications with sensitivity to the PTT model parameters, which requires further exploration to generalise these effects across different fluid formulations, additive chemistries and flow conditions.

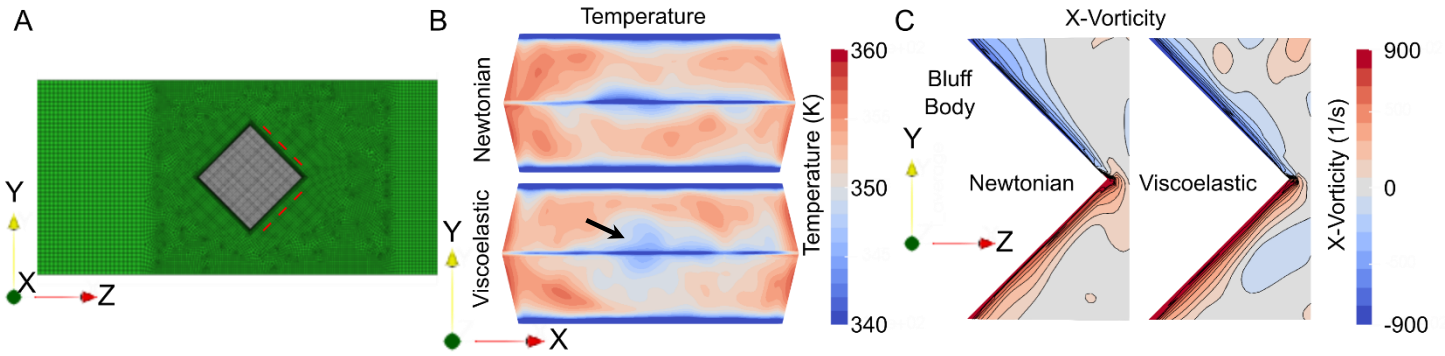

Fig. 5: (A) Representative images of the wake sides of the bluff body with time averaged (B) temperature and (C) X-vorticity profiles for both Newtonian and viscoelastic fluids. These illustrate the underlying processes leading to heat flux enhancement, stemming from the average increase in vorticity in the vicinity of the bluff body in the viscoelastic case and the disruption of the boundary layer locally.

The difference in heat transfer enhancement can be demonstrated more directly by plotting time-averaged temperature and vorticity plots on the downstream surfaces of the bluff body, as annotated in Figure 5A. The viscoelastic fluid is seen to have lower average temperatures in the centre (black arrow) and end edges of the bluff body, refer to Figure 5B. The origin of these lower temperatures can be traced to differences in the vorticity profiles between the Newtonian and viscoelastic fluids. As seen in Figure 5C, the average vorticity of the viscoelastic fluid in the vicinity of the bluff body is stronger than in the Newtonian fluid as more vortical structures can be detected in the vicinity also modifying the topology of the boundary layers forming on the two wake sides of the bluff body, as highlighted by the vorticity isolines in the vicinity of bluff body.

4. Conclusion

This study illustrates the potential of viscoelastic fluids to enhance heat transfer and modify vortex structures in wall bounded flows, with applications to immersion cooling systems. Through computational simulations validated by experiments, we show that the PTT model captures the essential nature of viscoelastic flows and how the model parameters affect the interplay between inertial and elastic forces. Our findings show that viscoelastic fluids enhance the vorticity of secondary flows and show a trending increase in heat transfer with increasing Reynolds number. Of course, owing to the interplay of elastic and inertial forces, careful optimisation of the fluid rheology, including normal stress difference ratio, flow conditions and geometrical layout is necessary to maximise viscoelasticity-induced heat transfer enhancement.

Acknowledgements

The work has received funding from the EU Framework Programmes for Research and Innovation HORIZON 2020 and Horizon Europe under the grant agreements No. 899659 (I-BAT project) and No. 101130315 (E-COOL project).

References

[1] C. Roe, X. Feng, G. White, R. Li, H. Wang, X. Rui, C. Li, F. Zhang, V. Null, M. Parkes, and Y. Patel, "Immersion cooling for lithium-ion batteries – A review," *J Power Sources*, vol. 525, p. 231094, 2022.

[2] T. G. Tranter, R. Timms, P. R. Shearing, and D. J. L. Brett, "Communication—Prediction of Thermal Issues for Larger Format 4680 Cylindrical Cells and Their Mitigation with Enhanced Current Collection," *J Electrochem Soc*, vol. 167, no. 16, p. 160544, 2020.

[3] W. Wu, S. Wang, W. Wu, K. Chen, S. Hong, and Y. Lai, "A critical review of battery thermal performance and liquid based battery thermal management," *Energy Convers Manag*, vol. 182, pp. 262–281, 2019.

[4] X. Na, H. Kang, T. Wang, and Y. Wang, "Reverse layered air flow for Li-ion battery thermal management," *Appl Therm Eng*, vol. 143, pp. 257–262, 2018.

[5] S. Gota, C. Huizenga, K. Peet, N. Medimorec, and S. Bakker, “Decarbonising transport to achieve Paris Agreement targets,” *Energy Effic*, vol. 12, no. 2, pp. 363–386, 2019.
[6] T. Tan, L. Rennels, and B. Parthum, “The social costs of hydrofluorocarbons and the benefits from their expedited phase-down,” *Nat Clim Chang*, vol. 14, no. 1, pp. 55–60, 2024.
[7] Q. Wang, B. Jiang, B. Li, and Y. Yan, “A critical review of thermal management models and solutions of lithium-ion batteries for the development of pure electric vehicles,” *Renewable and Sustainable Energy Reviews*, vol. 64, pp. 106–128, 2016.
[8] T. Wang, K. J. Tseng, and J. Zhao, “Development of efficient air-cooling strategies for lithium-ion battery module based on empirical heat source model,” *Appl Therm Eng*, vol. 90, pp. 521–529, 2015.
[9] S. Chakraborty, D. Shukla, and P. Kumar Panigrahi, “A review on coolant selection for thermal management of electronics and implementation of multiple-criteria decision-making approach,” *Appl Therm Eng*, vol. 245, p. 122807, 2024.
[10] D. A. Siginer and M. F. Letelier, “Heat transfer asymptote in laminar flow of non-linear viscoelastic fluids in straight non-circular tubes,” *Int J Eng Sci*, vol. 48, no. 11, pp. 1544–1562, 2010.
[11] C. G. Speziale, “On the development of non-Newtonian secondary flows in tubes of non-circular cross-section,” *Acta Mech*, vol. 51, no. 1, pp. 85–95, 1984.
[12] L. Xi, “Turbulent drag reduction by polymer additives: Fundamentals and recent advances,” *Physics of Fluids*, vol. 31, no. 12, 2019.
[13] V. Steinberg, “Elastic turbulence: an experimental view on inertialess random flow,” *Annu Rev Fluid Mech*, vol. 53, no. 1, pp. 27–58, 2021.
[14] D.-Y. Li, X.-B. Li, H.-N. Zhang, F.-C. Li, S. Qian, and S. W. Joo, “Efficient heat transfer enhancement by elastic turbulence with polymer solution in a curved microchannel,” *Microfluid Nanofluidics*, vol. 21, pp. 1–13, 2017.
[15] B. A. Toms, “Some observations on the flow of linear polymersolutions through straight tubes at large Reynolds numbers,” in *Proc. 1st Intl Congr. Rheol.*, 1949, pp. 135–141.
[16] Y. Dubief, V. E. Terrapon, and B. Hof, “Elasto-inertial turbulence,” *Annu Rev Fluid Mech*, vol. 55, no. 1, pp. 675–705, 2023.
[17] F. Pimenta and M. A. Alves, “Stabilization of an open-source finite-volume solver for viscoelastic fluid flows,” *J Nonnewton Fluid Mech*, vol. 239, pp. 85–104, 2017.
[18] N. P. Thien and R. I. Tanner, “A new constitutive equation derived from network theory,” *J Nonnewton Fluid Mech*, vol. 2, no. 4, pp. 353–365, 1977.
[19] R. Jesudasan and J.-D. Müeller, “High-Resolution CAD-Based Shape Parametrisation of a U-Bend Channel,” *Aerospace*, vol. 11, no. 8, p. 663, 2024.
[20] G. Noetscher and R. Charles, “Benchmarking bluff body aerodynamics,” in *21st AIAA Aerodynamic Decelerator Systems Technology Conference and Seminar*, 2011, p. 2607.
[21] R. Fattal and R. Kupferman, “Constitutive laws for the matrix-logarithm of the conformation tensor,” *J Nonnewton Fluid Mech*, vol. 123, no. 2–3, pp. 281–285, 2004.
[22] L. L. Ferrás, M. L. Morgado, M. Rebelo, G. H. McKinley, and A. M. Afonso, “A generalised Phan–Thien—Tanner model,” *J Nonnewton Fluid Mech*, vol. 269, pp. 88–99, 2019.
[23] M. F. Tomé, G. S. Paulo, F. T. Pinho, and M. A. Alves, “Numerical solution of the PTT constitutive equation for unsteady three-dimensional free surface flows,” *J Nonnewton Fluid Mech*, vol. 165, no. 5, pp. 247–262, 2010.
[24] H. Knauss, T. Roediger, D. A. Bountin, B. V Smorodsky, A. A. Maslov, and J. Srulijes, “Novel sensor for fast heat flux measurements,” *J Spacecr Rockets*, vol. 46, no. 2, pp. 255–265, 2009.
[25] L. Weiss, I. Karathanassis, B. Rueppel, T. Smith, and M. Wensing, “Enhancing Heat Transfer in Immersion Cooling of Battery Packs-Using ALTP Heat Flux Sensors,” *SAE Technical Paper*, 2024.
[26] Y. Saffar, S. Kashanj, D. S. Nobes, and R. Sabbagh, “The physics and manipulation of Dean vortices in single-and two-phase flow in curved microchannels: A review,” *Micromachines (Basel)*, vol. 14, no. 12, p. 2202, 2023.
[27] T. Hayat, A. M. Siddiqui, and S. Asghar, “Some simple flows of an Oldroyd-B fluid,” *Int J Eng Sci*, vol. 39, no. 2, pp. 135–147, 2001.
[28] M. A. Alves, F. T. Pinho, and P. J. Oliveira, “Study of steady pipe and channel flows of a single-mode Phan-Thien–Tanner fluid,” *J Nonnewton Fluid Mech*, vol. 101, no. 1, pp. 55–76, 2001.
[29] W. M. Jones, D. E. Marshall, and P. C. Walker, “The flow of dilute aqueous solutions of macromolecules in various geometries. II. Straight pipes of circular cross-section,” *J Phys D Appl Phys*, vol. 9, no. 5, p. 735, 1976.

[30] N. Burshtein, K. Zografos, A. Q. Shen, R. J. Poole, and S. J. Haward, "Inertioelastic Flow Instability at a Stagnation Point," *Phys Rev X*, vol. 7, no. 4, p. 41039, Nov. 2017.
[31] I. K. Karathanassis E. Pashkovski, M. Heidari-Koochi, H. Jadidbonab, T. Smith, M. Gavaises, and C. Bruecker, "Non-Newtonian flow of highly-viscous oils in hydraulic components," *J Nonnewton Fluid Mech*, vol. 275, p. 104221, 2020.
[32] S. G. Hatzikiriakos, G. Heffner, D. Vlassopoulos, and K. Christodoulou, "Rheological characterization of polyethylene terephthalate resins using a multimode Phan-Tien-Tanner constitutive relation," Rheol Acta, vol. 36, pp. 568–578, 1997.
[33] C. M. White and M. G. Mungal, "Mechanics and prediction of turbulent drag reduction with polymer additives," *Annu. Rev. Fluid Mech.*, vol. 40, no. 1, pp. 235–256, 2008.